Geological Field Trips

UHP eclogite and garnet ultramafic rock in the Cuaba Unit, Rio San Juan Metamorphic Complex, Dominican Republic

11th International Eclogite Conference, Rio San Juan, Dominican Republic, 30 January – 7 February 2015
Post-conference excursion: 7 February 2015

UHP eclogite and garnet ultramafic rock in the Cuaba Unit, Rio San Juan Metamorphic Complex, Dominican Republic

Richard N. ABBOTT, Jr.[1] & Grenville DRAPER[2]

(1)   Department of Geology, Appalachian State University, Boone, NC, 28608 USA.
(2)   Department of Earth Sciences, Florida International University, Miami, FL, 33199 USA.

PREFACE: Substantial parts of this report were paraphrased, excerpted or otherwise borrowed from Abbott & Draper (2013). For this, we graciously acknowledge authorization to do so from the editorial team of Geologica Acta. We thank you.

Cover image – Rio Cuaba (2008, Caribbean Geological Conference). This is part of **Stop 1** on this field trip. The boulders are of garnet peridotite, assemblage III: clinopyroxene + olivine + garnet + spinel + (retrograde hornblende + serpentine).

INDEX

1. Introduction

At the time of its discovery (Abbott & Draper, 1998; Abbott et al., 2001) the UHP rocks in the Cuaba unit of the Rio San Juan complex in the Dominican Republic was the second in the Americas. The first discovery was in the Seward Peninsula, Alaska (Till, 1981; Liebermann & Till, 1987). Today, there are at least two other UHP locations in the Americas, one in eastern Brazil (Parkinson et al., 2001) and the suggestion of an occurrence in the Canadian part of the North American Cordillera (MacKenzie et al., 2005).

The UHP rocks in the Cuaba unit are unusual for a number of reasons. They were delivered to the surface at an ocean-ocean convergent plate boundary, confounding mechanisms of uplift involving buoyancy (e.g., Gorczyk et al., 2007). One of the ultramafic rock types, garnet clinopyroxenite, contains the first described orogenic occurrence of coexisting garnet+spinel+corundum in the form of sub mm-scale inclusions of corundum and spinel in garnet (Abbott et al., 2005, 2006b; Gazel et al., 2012). Otherwise, naturally coexisting garnet+spinel+corundum is known only from rare alkremite and corgaspinite xenoliths in kimberlite (De Hoog, 2012). Laboratory experiments (Ackermand et al., 1975) show that the combination garnet+spinel+corundum is only possible at very high pressures (Abbott et al., 2005, 2006b; Gazel et al., 2011; Abbott & Draper, 2013). Finally, the ultramafic rock offers an unusually detailed picture of magmatic processes in the mantle.

The objective of the field trip is to examine evidence for UHP conditions at two stops in the Cuaba unit. Stop 1 features retrograded eclogite (in situ and in stream boulders) and garnet peridotite (in stream boulders). Stop 2 features a dike of clinopyroxenite garnetite cutting a 5-meter boulder of olivine clinopyroxenite.

Abbreviations for minerals and mineral components follow the convention of Kretz (1983) and Whitney & Evans (2010). Abbreviations for minerals are capitalized, e.g., Cpx, Grt, etc.; abbreviations for components of a mineral are not capitalized, e.g., di in Cpx, prp in Grt, etc. Neither Kretz (1983) nor Whitney & Evans (2010) provide abbreviations for three important pyroxene components. We therefore define the following abbreviations: Ca-ts = $CaAl_2SiO_6$ (Ca-tschermak component), Al-buf = $CaMg_{1/2}Ti_{1/2}AlSiO_6$ (Al-buffonite component); Ca-esk = $[]_{1/2}Ca_{1/2}AlSi_2O_6$ (Ca-eskola component).

Legend:

Pleistocene - Holocene
- Undifferenciated deposits

Late Miocene - Pliocene
- Haitises Limestones and Villa Trina Fms

Lower/Middle Miocene
- Piragua Conglomerates

Middle/Late Eocene - Oligocene
- La Toca Fm. Siliciclastic turbidites

Paleocene - Middle Eocene
- Imbert Fm. Lower-Middle Eocene
- Olistostrome

Río San Juan Complex

Río Boba Metaplutonic Complex
- La Manaclá Hbl-gabbros, diorites and tonalites
- Matel oxide-gabbronorites and metagabbronorites
- Quita Espuela metagabbronorites (two-pyroxene granulites)
- Ultramafic cumulates (wehrlites and websterites)

Morrito Unit
- El Guineal felsic schists
- Puerca Gorda mafic schists

Cuaba Mafic-Ultramafic Unit

Mafic rocks
- Jobito Sub-Unit. Amphibolites and mafic schists (SL-fabric)
- Guaconejo Sub-Unit. High-P Grt-Ep amphibolites and (coronitic) eclogites
- Banded metagabbros and metadiorites (variably sheared and retrogresed)

Ultramafic rocks (lenses)
- Grt-hornblende pyroxenite and garnet hornblendite (metacumulates)
- Serpentinized harzburgites and minor dunites

Helechal Serpentinized Peridotites
- Serpentinized spinel-harzburgites and lherzolites

Jagua Clara mélange
- Hicotea mafic schists
- Eclogite and blueschist blocks
- Serpentinitic (antigorite)-schists and gouge

Gaspar Hernández Serpentinites
- Massive and serpentinized harzburgites

GEOLOGICAL AND STRUCTURAL MAP
OF RÍO SAN JUAN COMPLEX
NORTHERN DOMINICAN REPÚBLIC
(Escuder-Viruete et al., 2013)

10 kms

Field trip stops: ① **Eclogite and Garnet-Peridotite**
② **Clinopyroxene-Garnetite Dike in Olivine-Clinopyroxenite**

Fig. 1. – Geology of the Rio San Juan complex (Escuder-Viruete et al., 2013). Movement between the North American Plate and Caribbean Plate is accommodated by the Septentrional Fault, Camu Fault zone (CFZ) and an offshore strongly oblique convergent zone (Jansma et al., 2000; Mann et al., 2002). Field trip stops are indicated. The Cuaba unit is intruded by the Rio Boba metaplutonic complex.

All thermodynamic calculations using the computer program THERMOCALC were done with version tc325, data set 5.5, 12 November 2004 (Holland & Powell, 1998; Powell et al., 1998; Powell, 2005). Henceforth, the program is referred to simply as THERMOCALC.

2. Geologic setting

The Cordillera Septentrional forms the landscape north of the Septentrional Fault in the Dominican Republic. The WNW-ESE trending range consists of Upper Eocene to Lower Miocene siliciclastic and carbonate sedimentary rocks, underlain by a basement of metamorphic and igneous rocks (Eberle et al., 1982; Lewis & Draper, 1990). The basement is exposed in a number of stratigraphic windows, or "inliers" where the cover has been eroded away. The largest of these inliers exposes the Rio San Juan (RSJ) metamorphic complex (Eberle et al., 1982; Draper & Nagle, 1991). Escuder-Viruete et al. (2009, 2011, 2013a,b) offer a detailed map of the RSJ complex (Fig. 1).

The RSJ complex (Draper & Nagle, 1991, Escuder-Viruete et al., 2009, 2011, 2013a,b) is divided into distinct northern and southern parts, which were juxtaposed by faulting, probably in the Paleogene (Draper & Nagle, 1991; Draper et al., 1994). The northern part of the inlier consists of serpentinite and blueschist-eclogite melange with serpentine matrix, faulted against fine-grained, coherent greenschist-blueschist facies rocks. The HP/low temperature (LT) metamorphism of these rocks is interpreted as having resulted from SW-directed subduction in the Cretaceous (Draper & Nagle, 1991; Draper et al., 1994; Krebs et al., 2008, 2011). The southern part of the RSJ metamorphic complex consists of the Cuaba unit and the Rio Boba metaplutonic complex (Fig. 1). The Cuaba unit is predominantly hornblende gneiss and hornblende schist. The common mineral assemblage is Hbl+Pl(andesine)+Qtz+Rt+/-Grt+/-Bt+/-Ep. Draper & Nagle (1991) and more recently Escuder-Viruete et al. (2011, 2013a,b) indicate a mafic protolith (basalt/diabase/gabbro) of ocean-crustal origin (MORB).

Retrograded eclogite in the Guanejo sub-unit (Fig. 1) of the Cuaba unit was first reported in 1998 (Abbott & Draper, 1998). Evidence for eclogite is in the form of Pl-Di symplectite + Grt, with greater or lesser amounts of hornblende depending on the extent of retrograde hydration (Abbott & Draper, 1998, 2002, 2007, 2013). The retrograded eclogite occurs as mm- to dm-scale layers in otherwise symplectite-free hornblende gneiss. Garnet peridotite was first reported in 2001 (Abbott et al., 2001). The garnet peridotite, other garnet-bearing ultramafic rocks, and related olivine clinopyroxenite, occur as stream boulders that have weathered out of the Guanajeo sub-unit. The Cuaba unit was intruded by gabbroic to

6

quartz dioritic rocks of the Rio Boba metaplutonic complex (Draper & Nagle, 1991). The petrogenetic relationship (if any) between the HP/LT rocks in the northern part of the inlier and HP/UHP rocks of the Cuaba unit remains unclear.

3. Ultramafic rock

Garnet ultramafic rock and related olivine clinopyroxenite are of plutonic, igneous origin (Fig. 2, dikes, pegmatitic mineral segregations, cumulate texture) and document a series of mineral assemblages related by fractional crystallization (Abbott et al., 2005, 2006b, 2007; Gazel et al., 2011; Abbott & Draper, 2013). Except for one deeply weathered *in situ* exposure, all observations and samples of the ultramafic rock come from stream boulders. Field relationships inferred from the boulders (Fig. 2) indicate the following sequence of mineral assemblages, from oldest (high temperature) to youngest (low temperature):

I.   Olivine clinopyroxenite (Fig. 2a):
          Cpx + Ol + Opx + Mag + (retrograde Cr-Spl + Hbl + Srp),
II.   Garnet olivine clinopyroxenite:
          Cpx + Ol + Grt + (retrograde Hbl + Srp),
III.   Garnet peridotite:
          Cpx + Ol + Grt + Spl + (retrograde Hbl + Srp) (Fig. 2b),
IV.   Garnet clinopyroxenite (Fig. 2c) and dikes of clinopyroxene garnetite (Fig. 2a):
          Cpx + Grt + Spl + (retrograde Hbl),
V.   Corundum-bearing garnet clinopyroxenite (Fig. 2d) and irregular segregations of clinopyroxenite garnetite (Fig. 2c):
          Cpx + Grt + Spl + Crn + (retrograde Hbl).

The compositions of spinel and earliest-formed garnet retain some memory of near solidus conditions (Gazel et al., 2011, 2012). The Mg# for the earliest garnet and the Mg# for spinel both decrease (Fig. 2) from the garnet peridotite (III) to corundum-bearing garnet clinopyroxenite (IV), consistent with increasing Fe/Mg during fractional crystallization. Assemblages III, IV and V were referred to as (1), (2) and (3), respectively (Fig. 2) in Abbott et al. (2005, 2006b), before the discovery of assemblage I and inferred assemblage II (Abbott et al., 2007).

Rhythmic layering in the olivine clinopyroxenite (I) summons the possibility that a well-defined magma chamber can exist in the asthenosphere, a magma chamber complete with internally (perhaps convectively) circulating magma. The image closely resembles the model proposed by Sen at al. (2005) and Keshav et al. (2007) for the lower lithosphere beneath the island of Hawaii.

V(3)	(d)	Crn-bearing Grt clinopyroxenite
		Cpx+Grt+Spl+Crn, $Mg\#_{Grt}=34$, $Mg\#_{Spl}=44$
IV(2)	(c)	Grt clinopyroxenite & Cpx garnetite
		Cpx+Grt+Spl
III(1)	(b)	Grt peridotite
		Grt+Ol+Cpx+Spl, $Mg\#_{Grt}=50$, $Mg\#_{Spl}=64$
II		Grt Ol clinopyroxenite
		Cpx+Ol+Grt
I	(a)	Ol clinopyroxenite
		Cpx+Ol+Opx

(a) Stop 2   2 cm

(b) Stop 1   5 cm

(c)   2 cm

(d)   2 cm
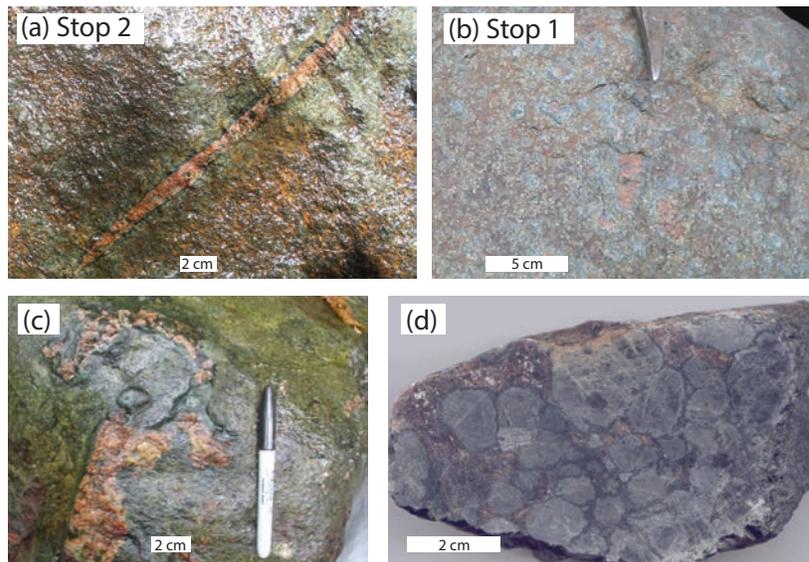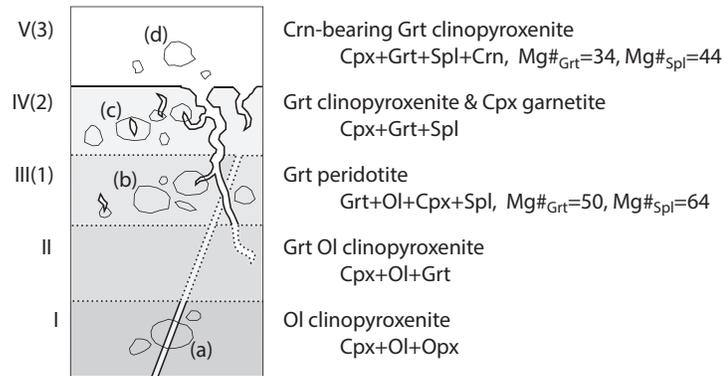
Fig. 2. – Schematic intrusive relationships (Abbott et al., 2007). Observed contacts are solid; inferred contacts are dotted. Irregular, closed loops are meant to represent the different kinds of boulders. The relative dimensions of the various features are not drawn to any particular scale. Boulders range in size up to 5m. Veins and segregations of corundum-bearing garnet clinopyroxenite, assemblage V, are typically on a decimeter scale. Straight dikes of garnet clinopyroxenite, assemblage IV, range in width up to 4 cm. **(a)** Narrow dike of clinopyroxenite garnetite (assemblage IV, Grt+Cpx+Spl+late Hbl) cutting olivine clinopyroxenite (assemblage I, Cpx+Ol+Opx+late Hbl+late Srp). Note the dark, ~2-mm selvage of late hornblende at the margins of the dike. **(b)** Garnet peridotite (assemblage III, Grt+Ol+Cpx+Spl+late Srp). **(c)** Pegmatitic segregation of corundum-bearing clinopyroxenite garnetite (assemblage V, Cpx+Grt+Spl+Crn) in garnet-clinopyroxenite (assemblage IV, Cpx+Grt+Spl). **(d)** Corundum-bearing garnet clinopyroxenite (DR03-12, assemblage V, Cpx+Grt+Spl+Crn+late Hbl). The dominant features of the rock are megacrysts of orthocumulate clinopyroxene (light gray euhedral to subhedral phenocrysts) and interstitial garnet. Spinel occurs as fine (<1 mm), inclusions in garnet. The fine, white inclusions in garnet are corundum. Hornblende forms thin (1 mm) selvages on phenocrysts of clinopyroxene.

3.1   Magmatic conditions

The original estimates of magmatic conditions (P >3.2 GPa and T >1550 °C, Abbott et al., 2005, 2006b, 2007) were based on experimental determinations in two simple systems, relating respectively to the following:

(1) The stability of sapphirine at high pressure. The sapphirine-out reaction Spr = Grt + Spl + Crn in the MAS system (Ackermand et al., 1975) defines the minimum pressure for the observed assemblage Grt+Spl+Crn.
(2) The solidus for garnet peridotite and garnet clinopyroxenite. High pressure (3 GPa) melting experiments in the CMAS system (Milholland & Presnall, 1998) show a field of stability for sapphirine, which at higher pressure must disappear where the solidus intersects the sapphirine-out reaction.

The minimum P-T conditions for melt coexisting with Grt+Spl+Crn(+Cpx) correspond to the intersection of the garnet clinopyroxenite (+Spl+Crn) solidus and the sapphirine-out reaction, Spr = Grt + Spl + Crn (Abbott et al., 2005, 2006b, 2007; Abbott & Draper, 2013; Gazel et al., 2011). In the CMAS system, the conditions at this intersection are P ~3.4 GPa, T ~1550 °C.

The influence of non-CMAS components (esp., Fe and Na) was explored in Gazel et al. (2011), who offered revised solidus conditions of P >3.2 GPa and T >1500 °C (filled circle in Fig. 3a), a little lower in P and T than the original estimates. The revised conditions take into account non-MAS components in the sapphirine-out reaction, and use the experimentally determined solidus for natural compositions of peridotite/clinopyroxenite (Walter, 1998; Herzberg et al., 2000; Hirschman, 2000).

Fe-Mg partitioning between spinel and garnet coexisting with olivine (Abbott et al., 2007; Gazel et al., 2012) is consistent with temperatures as high as ~1340 °C.

3.2   Phase relationships

The composition of the melt evolved in a systematic fashion (Fig. 3b) consistent with experimentally determined phase relationships (Milholland & Presnall, 1998), as modified by Abbott et al. (2005, 2006b) for P >3.2 GPa (see also, Abbott et al., 2007; Gazel et al., 2011; Abbott & Draper, 2013). Figure 3b shows liquidus relationships in part of the CMAS system defined by Di-Qtz-Fo-An, emphasizing liquids coexisting with garnet and clinopyroxene. Also illustrated is the liquid-line-of-descent consistent with the observed sequence of minerals assemblages. Details of the

derivation of the phase relationships are in Abbott et al. (2005, 2006b, 2007).
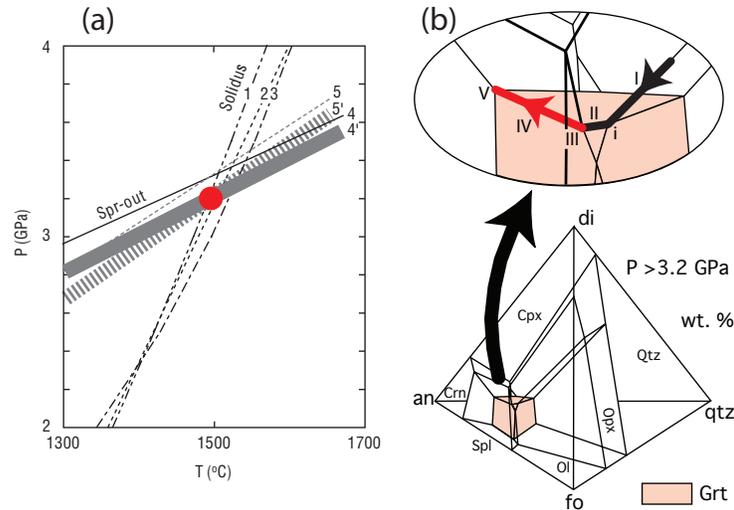
Fig. 3. – **(a)** Minimum P-T conditions for garnet peridotite magma (Gazel et al., 2011). The estimate of the minimum P-T conditions (filled circle, ~3.2 GPa, ~1500 °C, Gazel et al., 2011) takes into account the effects of non-CMAS components and tschermak substitution. Experimentally determined garnet peridotite solidus: 1 = Hirschmann (2000), 2 = Walter (1998), 3 = Herzberg et al. (2000). Experimentally determined sapphirine-out reaction: 4 (solid line) = sapphirine of composition $Mg_4Al_8Si_2O_{20}$ in the MAS system (Ackermand et al., 1975), and 4' (wide, solid band) = adjusted for Mg# of hypothetical sapphirine coexisting with the observed composition of spinel. THERMOCALC results for sapphirine-out reaction: 5 (dashed) = sapphirine of composition $Mg_{3.5}Al_9Si_{1.5}O_{20}$, and 5' (wide, dashed band) = adjusted for hypothetical Mg# of sapphirine coexisting with the observed composition of spinel. **(b)** Primary liquidus volumes for mineral-phases in a portion of the CMAS system at P > 3.4 GPa (Abbott et al., 2005, 2006b, 2007, as modified from Milholland & Presnall, 1998). Primary liquidus volume for garnet is highlighted. Details emphasizing liquids saturated with clinopyroxene are shown in the inset. Liquids on the bold line correspond to minerals assemblages I, II, III, IV and V, as indicated. Point "i" marks the Liq in the equilibrium, Ol + Cpx + Grt = Opx + Liq. Segment II is the locus of Liq in the equilibrium, Ol + Cpx + Grt = Liq. Point III marks the Liq in the equilibrium Cpx + Spl = Grt + Ol + Liq. Segment IV is the locus of Liq in equilibrium with Cpx, Grt and Spl. Point V marks the Liq in the equilibrium Cpx + Grt + Crn = Spl + Liq.The influence of non-CMAS components (esp., Fe and Na) was explored in Gazel et al. (2011), who offered revised solidus conditions of P >3.2 GPa and T >1500 °C (filled circle in Fig. 3a), a little lower in P and T than the original estimates. The revised conditions take into account non-MAS components in the sapphirine-out reaction, and use the experimentally determined solidus for natural compositions of peridotite/clinopyroxenite (Walter, 1998; Herzberg et al., 2000; Hirschman, 2000).

3.3 Three types of garnet

Abbott & Draper (2008, 2013) and Gazel et al. (2011) described three types of garnet in the garnet clinopyroxenite (Fig. 4, assemblage V, Cpx+Grt+Spl+Crn, sample DR03-12). The three types are compositionally and texturally distinct (Fig. 4a, b): Type-1 garnet, **Grt[1]**, 29<grs<33, Fe>Ca, adjacent to Spl+Crn; type-1' garnet, **Grt[1']**, 37<grs<47, Fe~Ca, away from Spl, Crn, Cpx and Hbl; and type-2 garnet, **Grt[2]**, 33<grs<42, Fe~Ca, associated with Hbl and Cpx. Phase relationships (Fig. 4c) modeled on 3-GPa experimental data (Abbott et al., 2005, 2006b, 2007; Gazel et al., 2011) show the following: The composition of **Grt[1]** is consistent with solidus or near solidus conditions, >3.2 GPa. The composition of **Grt[1']** is consistent with having formed isochemically from solidus or near solidus, high-Al clinopyroxene (Ca-ts ~0.5, i.e., approximately isochemical with Grt). **Grt[2]** formed late, under crustal conditions in conjunction with the formation of hornblende and final adjustments to the composition of clinopyroxene. The observed, low-Al clinopyroxene is interpreted as the reequilibrated cores of originally magmatic clinopyroxene (early crystallized, Ca-ts <0.5, i.e., less aluminous than garnet).

The three types of garnet are also distinct in terms REEs (Fig. 4d, and see Gazel et al., 2011). The REE data (Gazel et al., 2011) show distinct "humped" or "sinusoidal" REE patterns, typical of garnet from acknowledged UHP settings (i.e., garnet in kimberlite, and microinclusions of garnet in diamond). The peak of the "hump" in the normalized REE patterns for **Grt[1]** and **Grt[1']** is at Eu. The normalized REE patterns for **Grt[2]** show two peaks, at Sm and Gd on either side of Eu, such that the pattern has a small negative Eu anomaly on an otherwise upwardly convex pattern. The partitioning of REEs between **Grt[1']** and **Grt[1]** (Fig. 4d, 4th diagram) is consistent with the former having inherited its REEs from a high-Al clinopyroxene predecessor of UHP magmatic origin (Gazel et al., 2011, 2012). The partitioning plots close to experimental data for clinopyroxene-garnet REE partitioning at 1475 °C (3 GPa) (Tuff & Gibson, 2007), especially with regard to the average slope, $d(\mathbf{Grt[1']}/\mathbf{Grt[1]})/d$(atomic number). The **Grt[1']**/**Grt[1]** partitioning for the heavy (least mobile) REEs plot even closer to unity than the experimental data (Tuff & Gibson, 2007), suggesting temperatures higher than 1475 °C, i.e., approaching magmatic conditions at P >3 GPa (Gazel et al., 2011, 2012; Abbott & Draper, 2013).

Fig. 4. – Three types of garnet. **(a)** Photomicrograph of garnet-clinopyroxenite (DR03-12). Type-1 garnet, **Grt[1]** (far right), is not associated with clinopyroxene or hornblende. Type-1' garnet, **Grt[1']**, forms the bulk of the garnet, and is generally not associated with clinopyroxene or hornblende. Locally **Grt[1']** displays crystal faces. Type-2 garnet, **Grt[2]**, is associated with hornblende near clinopyroxene and is most conspicuously associated with hornblende as overgrowths on crystal faces of **Grt[1']**. **(b)** Chemistry of garnet and clinopyroxene, garnet-clinopyroxenite (DR03-12). Molar proportions of Mg, Ca and (Fe+Mn) in the three types of garnet and in clinopyroxene. For each mineral, the number of analyses is indicated in parentheses. **(c)** Chemical analyses of garnet and clinopyroxene superimposed on 3.5-GPa CMAS phase relationships (Abbott et al., 2005; Abbott & Draper, 2008; Gazel et al., 2011) inferred from 3.0-GPa experimental data (Abbott et al., 2005, 2006b). Compositions are projected from spinel onto the Al_2O_3-(Fe,Mn)SiO_3-$CaSiO_3$ plane. The subsolidus field for clinopyroxene (shaded) contracts dramatically with decreasing temperature, according to the temperature contours. Except for the solidus contour (1550 °C), the contour interval is 100 °C. The temperature-contours are based on 3-GPa experimental data: 1550 °C CMAS solidus (Abbott et al., 2005, 2006b), 1200 °C subsolidus contour (Boyd, 1970), and $CaAl_2SiO_6$ (tschermak clinopyroxene) (Hays, 1966). It is assumed that the clinopyroxene field is not significantly different up to 3.5 GPa. Solidus clinopyroxene can be very aluminous, stoichiometrically equivalent to garnet or even more aluminous (1550 °C). The straight red bar (with ends marked III and V) is the projected locus of liquids coexisting with garnet+clinopyroxene+spinel (assemblage IV) (Abbott et al., 2005). **Grt[1]** plots close to the composition of garnet coexisting with liquid+corundum+aluminous clinopyroxene. **Grt[1']** plots close to the composition of aluminous clinopyroxene coexisting with liquid+corundum+garnet. Chemical analyses of the observed clinopyroxene plot close to diopside-hedenbergite, within the 900 °C-field for subsolidus clinopyroxene. **(d)** Chondrite-normalized mineral REE data. (1st diagram) Clinopyroxene and **Grt[2]** (top diagram) from garnet-clinopyroxenite (DR03-12). For each mineral the average REE values are plotted (bold, solid line); maximum and minimum values bound the shaded region. Note the unusual negative Eu anomaly in the REE ratios for **Grt[2]**. (2nd diagram) **Grt[1]** and **Grt[1']** from the garnet-clinopyroxenite (DR03-12). For each mineral the average REE values are plotted (bold, solid line); maximum and minimum values bound the shaded region. (3rd diagram) UHP garnet, Sulu terrane, China (Zhang et al., 2004). Also shown are data for garnet from DR garnet peridotite (assemblage III, DR03-10). (4th diagram) REE partitioning between the average **Grt[1']** and the average **Grt[1]** of the garnet clinopyroxenite (DR03-12). Shaded regions represent high-temperature (1260-1380 °C) and low temperature (960-1080 °C) clinopyroxene-garnet REE partitioning from mantle xenoliths (Schmidberger & Francis, 2001). Also plotted are experimental data for clinopyroxene-garnet REE partitioning at 1475 °C (3 GPa) (Tuff & Gibson, 2007).

(a)

1 cm

Cpx

(b)

(molar proportions)

Mg

Assemblage V

Clinopyroxene
(n=16)

Grt[1]
(n=17)

Grt[2]
(n=42)

Grt[1']
(n=50)

Fe+Mn   Ca

(c)

+ Spinel
(molar proportions)

Al₂O₃
Corundum

Garnet
III IV V
Liq ~3.5 GPa
Clinopyroxene, n=16
Grt[1], n=17
Grt[1'], n=50

CaAl₂SiO₆
tschermak component

(Mg,Fe)₃Al₂Si₃O₁₂   Ca₃Al₂Si₃O₁₂

(Mg,Fe)SiO₃   CaSiO₃
Ca(Mg,Fe)Si₂O₆

1550
1500
1200

Olivine

(d)

Garnet-clinopyroxenite, DR03-12
Clinopyroxene
Grt[2]

Sample/Chondrite

La Ce Pr Nd Sm Eu Gd Tb Dy Ho Er Tm Yb Lu

Garnet-clinopyroxenite, DR03-12
Grt[1]
Grt[1']

Sample/Chondrite

La Ce Pr Nd Sm Eu Gd Tb Dy Ho Er Tm Yb Lu

UHP Garnet, Sulu
Garnet in garnet-peridotite, DR03-10

Sample/Chondrite

La Ce Pr Nd Sm Eu Gd Tb Dy Ho Er Tm Yb Lu

Low-T (870-1080 °C)
High-T (1260-1380 °C)
1475°C (3 GPa)

Clinopyroxene / Garnet

Grt[1'] / Grt[1]

La Ce Pr Nd Sm Eu Gd Tb Dy Ho Er Tm Yb Lu

13

3.4 Subsolidus P-T conditions

Temperatures were calculated (Abbott et al., 2006a) for Fe-Mg exchange between garnet and clinopyroxene in the garnet peridotite (III). Figure 5 shows the results for Ai's (1994) Fe-Mg exchange model, which agrees most closely with results from THERMOCALC. At 3.5 GPa, the calculated temperature is ~900 °C (Abbott et al., 2006a). The estimate temperature relates to subsolidus closure for Fe-Mg exchange between garnet and clinopyroxene.

Average P-T conditions were calculated for garnet peridotite (III, Ol+Grt+Cpx+Spl) using THERMOCALC. Details of the calculations are in Abbott & Draper (2013). The large, filled circle in Figure 5 marks the calculated conditions of P = 3.4 (+/-0.7) GPa and T = 838 (+/-170) °C, where the uncertainty expresses the standard deviation (error bars in Fig. 5). The conditions are consistent with approximately isobaric cooling from magmatic conditions.

Temperatures were also calculated for Fe-Mg exchange between garnet and hornblende, using the model of Graham & Powell (1984). The results are shown in Figure 5 as the vertical bar terminating at 2.5 GPa, the approximate upper pressure limit for hornblende (Abbott et al., 2007).

The UHP part of the envisioned P-T path (Fig. 5) involved approximately isobaric (P >3.2 GPa, e.g., 3.5 GPa) cooling from solidus conditions (~1500 °C) down to ~900 °C (Abbott et al., 2006a; Abbott & Draper, 2007, 2008, 2013; Gazel et al., 2011). At the subduction zone, the ultramafic rock was incorporated into, or otherwise mixed with, deep-subducted oceanic crust (eclogite). With regard to the UHP part of the path, we interpret the ultramafic rock as having been dragged to the subduction zone by forced convection in the mantle wedge (corner-flow), coupled with erosion of the hanging wall. Models of such forced convection (e.g., Gerya et al., 2002; Gorczyk et al., 2007; Roselle et al., 2002) suggest cooling at constant or increasing pressure.
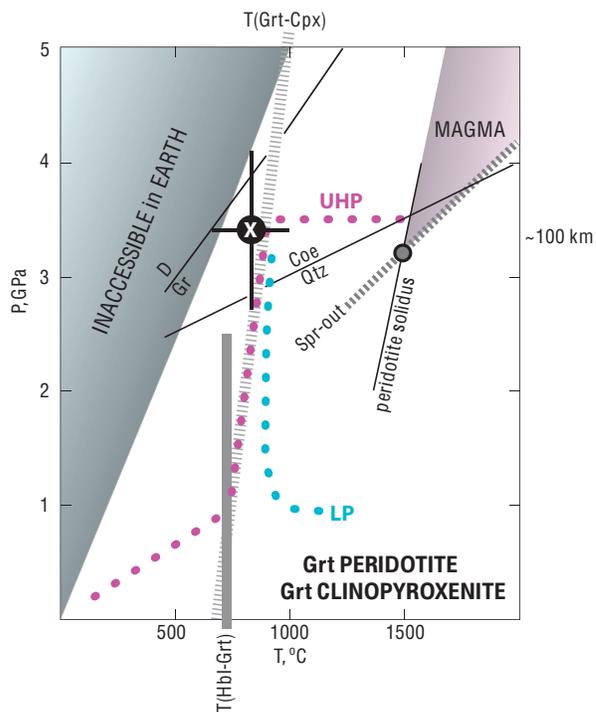
Fig. 5. – P-T conditions for garnet-bearing ultramafic rock and P-T path (magenta, dotted). The shaded pink region (P >3.2 GPa, T >1500 °C, Gazel et al., 2011) defines the magmatic conditions for the garnet ultramafic rock (Fig. 3a). The small, gray-filled circle marks the minimum P-T conditions (Fig. 3a). The large, filled circle "X" (with error bars, st. dev.) represents THERMOCALC results for the subsolidus equilibrium involving Grt+Spl+Cpx+Ol. Results of Cpx-Grt thermometry (Ai, 1994) are represented by the steep dashed band. Results of Grt-Hbl thermometry are represented by the vertical band terminating at ~2.5 GPa, the approximate upper pressure limit for hornblende. D/Gr, diamond-graphite; Coe/Qtz, coesite-quartz.

3.5   An alternative, low-pressure (LP) hypothesis

Hattori et al. (2009, 2010a) offer the alternative view that the garnet-bearing ultramafic rocks were derived from a plagioclase-bearing protolith of island-arc origin at relatively shallow depths (crust). In this low-pressure (LP) hypothesis, the garnet was the product of metamorphism during subduction. The proposed LP path is show in Figure 5. The LP model (Hattori et al., 2009, 2010a) was originally predicated on (1) a small positive Eu anomaly (Eu/Eu* =1.18-1.32) in the whole rock chemistry of two samples of garnet wehrlite (our garnet peridotite, III) and (2) the assumption that the trace element chemistry of the clinopyroxene relates to magmatic conditions. With regard to Eu, the thinking was that an Eu anomaly would signify involvement of plagioclase, hence crustal conditions. Subsequent data on four additional samples (Hattori et al., 2010b) are ambiguous. In fact, the least altered sample (lowest LOI) shows a small negative Eu anomaly (Eu/Eu* =0.89). It is worth noting that De Hoog (2012) acknowledges the ambiguity of the Eu anomaly, undermining Hattori's et al. (2009, 2010a, b) hypothesis, when he (De Hoog, 2012) states, "… bulk rock Eu anomalies are expected to be small or non-existent in these rocks [garnet peridotite], and thus the lack thereof provides no evidence as to UHT or LP origin." With regard to clinopyroxene, our work (Abbott & Draper, 2008, 2010; Gazel

et al., 2011) shows that the clinopyroxene is chemically equilibrated to late, retrograde crustal conditions (amphibolite facies). That is, the composition of the relict clinopyroxene (major elements and trace elements) no longer reflects magmatic conditions.

The LP model disregards the most compelling evidence for UHP magmatic origin (Abbott & Draper, 2010, 2013; Gazel et al., 2011) by ignoring basic phase relationships (albeit complex), orthocumulate clinopyroxene textures, structural evidence (dikes, cross-cutting mineral segregations), systematic variation in mineral assemblage (LLD), and systematic variations in compositions of relict minerals (esp., Grt, Spl). Hypothetical, monotonically increasing (light to heavy) REE ratios for garnet, used by Hattori et al. (2010a) in their modeling, and critical to their argument, bear absolutely no resemblance to the actual garnet (Gazel et al., 2011).

De Hoog (2012) commented on the UHP hypothesis, but none of his criticism precludes a UHP magmatic origin for the garnet ultramafic rocks (Gazel et al., 2012). The reader is referred to Gazel's et al. (2012) point-by-point reply to De Hoog's (2012) concerns. De Hoog (2012) did offer a means for improving the garnet-spinel thermometry (Gazel et al., 2012). The corrected, lower garnet-spinel temperatures, as high as 1340 °C (Gazel et al., 2012), are still prohibitively high for the LP model.

4. Eclogite

The typical eclogite (Fig. 6a, DR05-2) is granoblastic to subtly foliated, depending on the amount of hornblende. In hand specimen, the granoblastic texture consists of subhedral to euhedral porphyroblasts of deep-red garnet set in an aphanitic gray-green matrix. Garnet porphyroblasts are typically <3 mm, but can reach 7 mm. Hornblende occurs in narrow (~0.5 mm) selvages on the garnet and fills fractures in the larger garnets. Locally the hornblende is absent or scarce. The garnet porphyroblasts and matrix are in sub-equal proportions and collectively make up 85% or more of the rock.

Thin sections (Fig. 6a) reveal important microscopic details. The narrow hornblende selvages on garnet consist of an aphinitic intergrowth of hornblende, quartz and epidote. The matrix consists of fine-grained (0.01-0.05 mm) vermicular Pl-Cpx symplectite, referred to as type-I symplectite (Sym-I) in Abbott & Draper (2007). Minor minerals include Fe-Ti oxide, rutile, titanite, apatite, and pyrite. Titanite forms rims on the Fe-Ti oxide minerals. Small (~1 mm), isolated aggregates of fine-grained epidote (~10 modal %) occur sporadically throughout the matrix of type-I symplectite. The garnet contains micro inclusions of quartz, rutile, and

epidote. Hornblende is interpreted to be the last product of retrograde hydration. Prior to the formation of hornblende, the rock consisted of Grt+Sym+Qtz+Ep+Rt+Fe-Ti oxide. The inferred highest-grade assemblage was Grt+Omp+Ky+Coe+Rt+Fe-Ti oxide (Abbott & Draper, 2007).
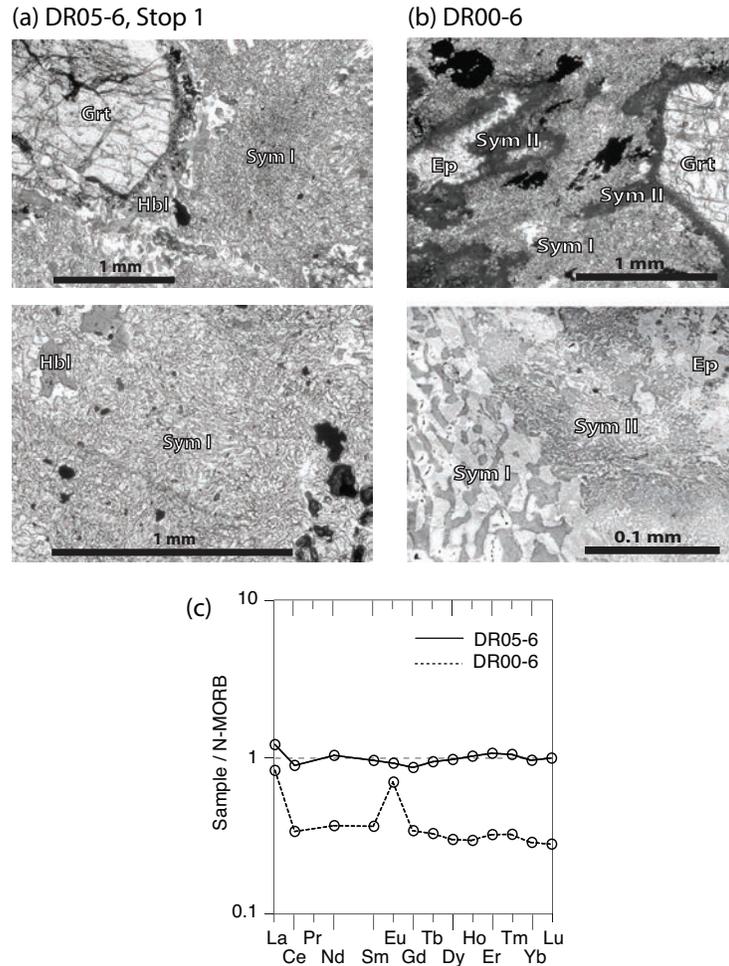
Fig. 6. – **(a)** Digital images of typical retrograded eclogite (sample DR05-2, plane polarized light). Porphyroblast of garnet rimmed by hornblende+quartz+plagioclase. The matrix consists of Pl-Cpx symplectite (Sym-I). **(a, lower)** Region of symplectite, showing the vermicular intergrowth of plagioclase and clinopyroxene. The opaque mineral is Fe-Ti oxide, rimmed by titanite. **(b)** Digital images of retrograded eclogite (sample DR00-6) with Pl-Cpx symplectite (Sym-I) and Pl-Ep symplectite (Sym-II). The garnet porphyroblast and aggregate of epidote (upper image) are each rimmed by optically amorphous symplectite-II (Pl-Ep). The matrix consists of Pl-Cpx symplectite (Sym-I). The opaque mineral is Fe-Ti oxide. **(b. lower)** SEM image showing Sym-I (Pl-Cpx) and Sym-II (Pl-Ep). **(c)** Whole-rock REE analyses, normalized to N-MORB (Sun & McDonough, 1989), for eclogite samples DR05-6 and DR00-6 (Abbott & Draper, 2013).

The most interesting manifestation of eclogite (Fig. 6b, DR00-6) differs from the typical eclogite in having a second kind of symplectite involving plagioclase and epidote, referred to as type-II sympectite (Sym-II) in Abbott & Draper (2007). Details become apparent in thin section (upper image, Fig. 6b) and in SEM images (lower image, Fig. 6b). Where hornblende is scarce, the gray-green matrix resolves into two types of symplectite. Symplectite-I (Sym-I) consists of a fine-grained (~0.05 mm) intergrowth of plagioclase and clinopyroxene. SEM images (lower image, Fig. 6b) reveal the second symplectite (Sym-II) to be an unusual intergrowth of microlaths (<0.005 mm) of epidote in plagioclase. The microsymplectite-II forms the narrow (~0.1 mm), optically amorphous mantles on garnet porphyroblasts and on aggregates of epidote (upper image, Fig. 6b). The contact between symplectite-I and microsymplectite-II is sharp (lower image, Fig. 6b). Symplectite-I (Pl-Cpx) touches neither garnet nor aggregates of epidote, by virtue of intervening microsymplectite-II (Pl-Ep). Minor minerals include quartz, Fe-Ti oxides, titanite, rutile, and zircon. Most of the quartz is associated with hornblende or occurs as inclusions in the garnet. Irregular crystals of Fe-Ti oxide occur in symplectite-I and are rimmed by titanite. Minute (<0.01 mm) crystals of rutile and zircon form scarce inclusions in garnet. Hornblende is interpreted as the last product of retrograde hydration, after the formation of symplectite-I and symplectite-II. Prior to the formation of hornblende, the rock consisted of Grt+Sym-I+Sym-II+Ep+Qtz+Rt+Fe-Ti oxide.

The two types of symplectite are believed to have formed from the decomposition of two types of omphacite, Omp-I from Sym-I (Pl-Cpx), and Omp-II from Sym-II (Pl-Ep). The compositions of the original omphacites were reintegrated (Abbott & Draper, 2007) from the components of the respective symplectites, acknowledging a wide range in the modal amount of plagioclase from 40% to 60% in each type of symplectite, and acknowledging observed variation in the composition of the plagioclase. The reintegrated composition for Omp-I is $(di+hd)_{45-30}$Ca-ts$_{4-1}$Al-buf$_{<1}$(jd+acm)$_{29-38}$Ca-esk$_{20-30}$(en+fs)$_{\sim1}$ with Mg#$_{Omp-I}$ 76-85; the reintegrated composition for Omp-II is $(di+hd)_{25-17}$Ca-ts$_{26-14}$Al-buf$_0$(jd+acm)$_{25}$Ca-esk$_{26-34}$(en+fs)$_{<1}$ with Mg#$_{Omp-II}$ ~14 (Abbott & Draper, 2007). Omp-I is unusual for its high content of Ca-esk, while Omp-II is unusual for its high content in Ca-ts and Ca-esk. The differences in the compositions suggest that Omp-I and Omp-II are related by an "immiscibility gap." While the situation is complicated by high values for Ca-ts and Ca-esk, the combined effects of which are not known, the difference in the (di+hd) values for Omp-I and Omp-II suggests that the gap may be related to well-known high-temperature immiscibility gap between (di-hd) and (en-fs) (Davidson & Lindsley, 1985). Perhaps, Ca-ts

and Ca-esk suppress the temperature of the "solvus." Alternatively, the compositional gap may be related to compositional gaps on the di-jd join (Davidson & Burton, 1987; discussed in Spear, 1993).

4.1 Rare Earth Elements

Whole rock chemical analyses were obtained for two samples of the retrograded eclogite (Abbott & Draper, 2013). The REE data are shown in Fig. 6, normalized to MORB (Sun & McDonough, 1989). Sample DR05-6 represents, both modally and texturally, the typical eclogite, differing little from sample DR05-2 (Fig. 6a). The major element chemistry of both rocks is consistent with low-K tholeiitic basalt in the IUGS classification system. DR05-6 is slightly quartz-normative, whereas DR00-6 is slightly olivine-normative. REE ratios for DR05-6 are all close to unity; hence, DR05-6 preserves a MORB signature. The data are consistent with the MORB-group in a more comprehensive trace-element data-set for rock samples from the same unit (Escuder-Viruete, 2009). Except for the strong positive Eu-anomaly, the REE pattern for DR00-6 mimics the pattern for DR05-6 but with systematically lower REE ratios. The strong positive Eu-anomaly suggests that DR00-6 was a plagioclase cumulate. The pattern can be modeled reasonably well as ~75% cumulate plagioclase and ~25% melt of the composition of N-MORB or DR05-6. The (Escuder-Viruete, 2009) also indicates an island-arc tholeiite (IAT) component in all three units of the Cuaba terrane.

4.2 P-T conditions for the eclogite

This section presents a summary of P-T estimates for eclogite sample DR00-6 (Abbott & Draper, 2007, 2013). Results are portrayed in Figure 7 and compared with the P-T path for the garnet peridotite (Fig. 5). For each of the equilibria represented in Figure 7, the range of conditions reflects the uncertainty, especially with regard to the inferred composition of the original omphacites, Omp-I and Omp-II (for details, see Abbott & Draper, 2007, 2013).

4.2.1 Grt-Cpx thermometry

Temperatures were calculated using Fe-Mg exchange between garnet and clinopyroxene. Figure 7 shows the range of temperature using Ai's (1994) Fe-Mg exchange model for garnet paired with clinopyroxene in Sym-I (Abbott & Draper, 2007, 2013).

THERMOCALC Fe-Mg exchange thermometry was applied to garnet paired with Cpx in Sym-I and to garnet paired with hypothetical Omp-I, at two pressures, 1.5 and 3.0 GPa (horizontal bars at these pressures in Fig. 7). The THERMOCALC temperatures (Grt-Omp and Grt-Cpx) overlap temperatures from Ai's (1975) model (Grt-Cpx), but the THERMOCALC

temperatures form a narrower range, displaced to lower temperature relative to results using Ai's (1994) model.   For the broad scale of conditions shown in Figure 7, the difference is not significant.

4.2.2 Estimation of pressure

Pressures were estimated from the intersections of the Grt-Cpx thermometry and the following equilibria:

(1) $ab^{Pl} = jd^{Omp} + Qtz$
(2) $15\ di^{Omp} + 12\ czo^{Ep} = 13\ grs^{Grt} + 5\ prp^{Grt} + 12\ Qtz + H_2O$
(3) $6\ czo^{Ep} = 4\ grs^{Grt} + 5\ Ky + Qtz + 3\ H_2O$
(4) $3\ di^{Omp} + 3\ Ca\text{-}ts^{Omp} = 2\ grs^{Grt} + prp^{Grt}$

None of the equilibria involves Fe-components, thus they are largely independent of problems related to uncertainty in the oxidation state of Fe.
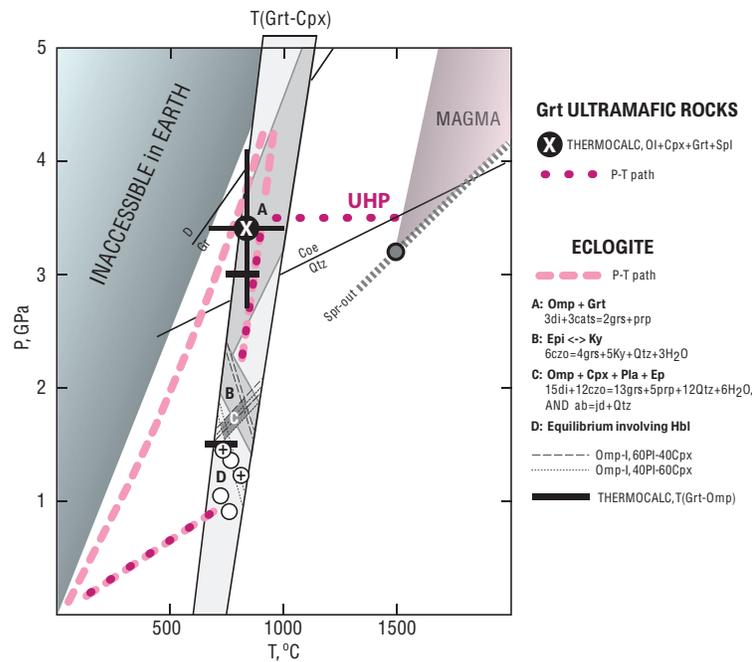
Fig. 7. – P-T estimates for eclogite based on garnet-clinopyroxene Fe-Mg exchange thermometry and other equilibria, described in the text. The proposed P-T path for the eclogite is shown by the bold, dashed, pink line. The proposed P-T path for the garnet-bearing ultramafic rock (Fig. 5) is shown as the bold, magenta dotted line. D/Gr, diamond-graphite; Coe/Qtz, coesite-quartz.

Equilibrium 1 was evaluated for hypothetical Omp-I paired with plagioclase. The calculations were referred to the extreme compositions of the type-I omphacite (Omp-I$_{40}$, reintegrated from 40% Pl + 60% Cpx, and Omp-I$_{60}$, reintegrated from 60% Pl + 40% Cpx) and extreme compositions for plagioclase. The restricted range of solutions is shown in Figure 7 as the positive-slope equilibria bounding the shaded region "C." Solutions to equilibrium 2 (negative-slope equilibria bounding shaded region "C") were evaluated for garnet, epidote (Abbott & Draper, 2007, 2013) and the extreme compositions for Omp-I (Omp$_{40}$-Omp$_{60}$). The intersection of solutions to equilibrium 1 and equilibrium 2 (stable conditions for Grt+Omp-I$_{40-60}$+Pl+Ep+Qtz+H$_2$O) defines the small P-T region labeled "C," P ~1.5-1.9 GPa and T ~700-850 °C.

Equilibrium 3 relates to the maximum pressure for the observed epidote (czo$_{25}$) and also relates to the pressure above which kyanite is possible. Solutions for equilibrium 3 are represented by the shaded region labeled "B" in Figure 7. The equilibrium is independent of omphacite and plagioclase, and suggests slightly higher pressure than equilibria 1 and 2. Evidently, the decomposition of Omp-I to Sym-I took place under conditions consistent with the stability of epidote. Inasmuch as Sym-II consists of plagioclase and epidote, Omp-II and Omp-I must have decomposed under similar conditions.

Equilibrium 4 explores the stable coexistence of Omp-I+Omp-II+Grt (Abbott & Draper, 2007, 2013). THERMOCALC solutions for equilibrium 4 reside in the region labeled "A" in Figure 7. The low-pressure limit corresponds to the solution involving Omp-I$_{47}$ (reintegrated from Sym-I$_{47}$ of 47% Pl + 53% Cpx) and Omp-II$_{40}$ (reintegrated from Sym-II$_{40}$ of 40% Pl + 60% Ep). The high-pressure limit corresponds to the solution involving Omp-I$_{57}$ (reintegrated from Sym-I$_{57}$ of 57% Pl + 43% Cpx) and Omp-II$_{60}$ (reintegrated from Sym-II$_{60}$ of 60% Pl + 40% Ep). All possible solutions involving intermediate, equilibrium pairs of Omp-I and Omp-II, coexisting with garnet, reside between these extremes. Most of region "A" is between the quartz-coesite equilibrium and the graphite-diamond equilibrium (~2.8 to ~4.4 GPa). The conditions compare favorably with subsolidus conditions for the garnet peridotite.

Finally, the "average P-T" option in THERMOCALC was used to estimate the equilibrium conditions for Hbl+Grt+Cpx+Pl+Qtz (open circles, Fig. 7), and for Hbl+Grt+Cpx+Ep+Pl+Qtz (circles with "+," Fig. 7). None of the equilibria involved H$_2$O.

The proposed P-T history for the eclogite is indicated by the pink, dashed path in Figure 7. The prograde history remains speculative, but is presumed to have started with cooled basalt on the sea floor. The proto-eclogite (sea floor basalt) was subducted to a depth as great as 120 km (~4 GPa). At the highest pressure, the assemblage would have been Grt+Omp-I+Ky+Coe+Rt+Fe-Ti oxide. The shaded region "A" relates to the retrograde assemblage, Grt+Omp-I+Omp-II+Ky+Coe+Rt+Fe-Ti oxide, and the formation of Omp-II according to a reaction of the form,

Omp-II + Coe = Omp-I + Ky +/- Grt.

Details of the reaction are given in Abbott & Draper (2007, 2013). The region "B" relates to the retrograde appearance of epidote and consumption of kyanite. Region "C" corresponds to the breakdown of Omp-I to Sym-I (Pl+Cpx), and must also correspond closely to the breakdown of Omp-II to Sym-II (Pl+Ep). Circles "D" relate to the formation of retrograde hornblende. The inferred P-T path involved (1) deep subduction of basalt to ~120 km (~4 GPa) and prograde metamorphism, (2) nearly adiabatic uplift to ~30 km (~1 GPa) and retrograde metmorphism, followed by (3) a final stage of uplift with accelerated cooling, perhaps mediated by H_2O, through crustal conditions. The sequence of retrograde mineral assemblages along the retrograde part of the dashed path in Figure 7 is illustrated in Figure 8 (from Abbott & Draper, 2007, 2013).
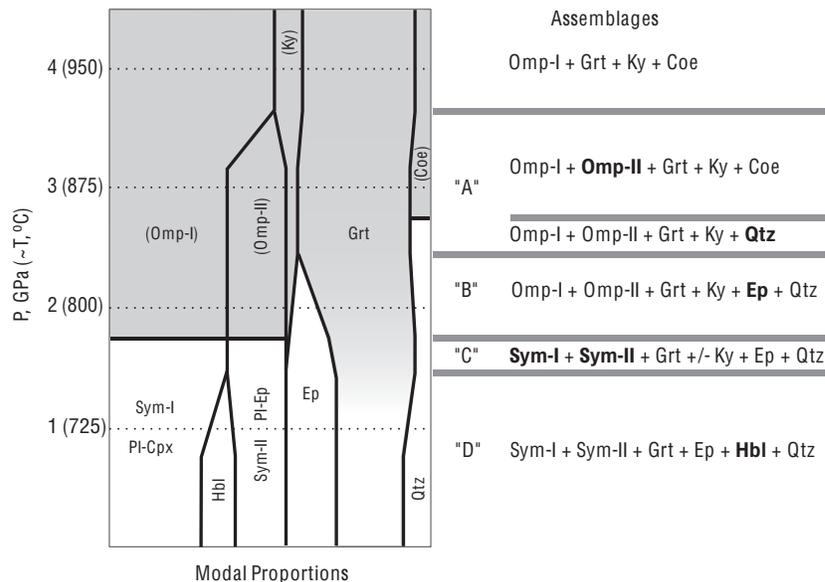
Fig. 8. – Evolution of the mineral assemblage in DR00-6 along the retrograde path designated by the bold, dashed pink line in Figure 7. Widths of the regions are qualitatively proportional to the modal amounts of the minerals.

The sequence of retrograde mineral assemblages (Figs. 7, 8) is broadly consistent with phase relationships calculated by Wei & Clarke (2011) for a "standard" MORB composition. The highest-grade mineral assemblages inferred for the Cuaba eclogite (P > region "B," Figs. 7, 8) correctly fall in Wei & Clarke's (2011) kyanite-eclogite field, but at temperatures higher than the maximum temperature of 700 °C considered by Wei & Clarke (2011). On the retrograde P-T path for the Cuaba eclogite (Figs. 7, 8), hornblende appears at a lower pressure than the decomposition of the omphacite (Omp-I) to Pl-Cpx symplectite (Sym-I). This means that the retrograde P-T path for the Cuaba eclogite passes directly from Wei & Clarke's (2011) kyanite-eclogite field to their amphibolite field, without passing through their hornblende-eclogite field.   This implies temperatures greater than 700 °C, outside the range of temperature considered by Wei & Clarke (2011). While the retrograde P-T path for the Cuaba eclogite is broadly consistent with Wei & Clarke's (2011) calculated phase diagrams, there are certain inconsistencies. For instance, in the region "B" in Figure 7 the maximum pressure for epidote is ~2.4 GPa at ~700 °C, whereas the maximum pressure for epidote in Wei & Clarke's (2011) kyanite-epidote field is ~2.5 GPa at ~650 °C. This discrepancy may reflect differences in fugacity of oxygen or activity of H_2O or both. Increased oxygen fugacity should expand the field for epidote to higher temperatures.

5. Tectonic model

The tectonic interpretation shown in Figure 9 (Abbott & Draper, 2013) serves as a working hypothesis. The isobaric part of the P-T path for the garnet ultramafic rock took place in the mantle and involved delivery to the subduction zone in mid to Late Cretaceous time (1, Fig. 9). Garnet ultramafic rock of the mantle wedge was cooled and introduced into the deep-subducted oceanic crust (1′, Fig. 9) in response to forced convection in the mantle wedge (corner flow) combined with erosion of the hanging wall of the subduction zone. The eclogite, with tectonic blocks of the garnet ultramafic rock onboard, was transported up the subduction channel (2, Fig. 9), perhaps by some variant of reverse flow as modeled for instance by Gerya et al. (2002) and Gerya & Yuen (2003). The mechanism is very poorly understood in the present context because of the great depths involved. Nevertheless, in an effort to explain the exhumation of the garnet peridotite in the Cuaba unit, Gorczyk et al. (2007) developed a numerical model involving the upwelling of hydrated peridotite and partially molten peridotite, which in turn induces the upwelling of hot, presumably dry asthenosphere. In their numerical simulation UHP material (Cuaba unit?) is introduced into, and transported

up, the subduction channel from depths as great as ~120 km (4 GPa). However, Krebs et al. (2011) point out that the constraints used in Gorczyk's et al. (2007) simulation involve unrealistically slow rates of convergence (~25 mm/a) and an unrealistically short duration of steady-state subduction (~18 Ma). Whatever the mechanism, transport up the subduction channel was essentially completed prior to mid-crustal intrusion by dioritic to gabbroic rocks (Rio Boba metaplutonic complex) of uncertain, but presumably Upper Cretaceous, age. The last part of the history relates to uplift through the crust to the surface (3, Fig. 9), completed by mid-Eocene, perhaps in response to initiation of transcurrent tectonics (Mann et al., 1990; Pindell & Barrett, 1990; Draper et al., 1994, 1996; Pindell et al., 2005, 2009).
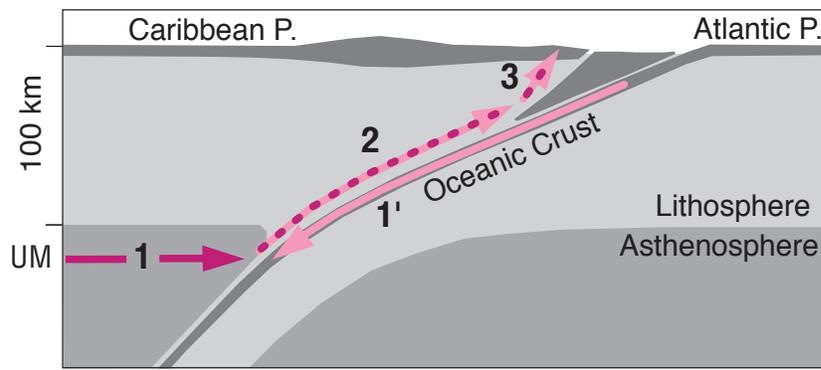
Fig. 9. – Simplified plate tectonic interpretation, showing the path for the eclogite (pink), and the path for the garnet ultramafic rock (magenta).

6. Conclusions

The great depth of origin of the garnet-bearing ultramafic rocks (>100 km) and REE patterns for the garnet implicate an origin in the mantle. The very high temperatures for protoliths of the garnet-bearing ultramafic rocks (~1500 °C) suggest that they are a product of mantle plume-head magmatism under UHP conditions (Gazel et al., 2011, 2012). Speculation favors the ancestral Galapagos plume (Kerr et al., 2003; Pindell & Kennan, 2009, Gazel et al., 2011).

Given the nature of forced convection (corner flow) in the mantle wedge (e.g., Gerya et al., 2002; Roselle et al., 2002), it is unlikely that the path of subsolidus cooling for the ultramafic rock could have escaped passing through the coesite field. Well away from the subduction zone, flow-lines in the mantle wedge are isobaric. Close to the subduction zone, flow-lines follow paths of increasing pressure in response to drag (draw-down) on the hanging wall of the subduction zone. Isobaric cooling all the way

to the subduction zone would require unrealistically rapid erosion of the hanging wall. Even for this limiting situation, cooling from the minimum conditions (~3.2 GPa, ~1500 °C) for the original ultramafic magma passes through the coesite field. For isobaric cooling, the ultramafic rock would have been incorporated into the eclogite at P >3.2G Pa and T >850 °C, well within the coesite field.

Subsolidus conditions related to near adiabatic decompression are the same for eclogite and the ultramafic rock. This supports the proposal that the ultramafic rock was delivered to the surface as tectonic blocks in the eclogite.

7. Acknowledgements

<center>**Itinerary**</center>

km

0.0 Intersection of RD132/RD19 in San Francisco de Macoris, proceed **NE** on RD19 (Calle Castillo) toward El Cercado/Cuevas.

9.0 Go left (**N**) at the village of Cuevas onto gravel road (~UTM E0375.7-N2138.3).
Proceed past two shallow-water fords to the end of the road.

11.0 Park at the end of the road.

Stop 1, Rio Cuaba: Proceed on foot upstream (**N**) by way of the trail on the east side of Rio Cuaba. The destination (~1 km) is a 2 meter-high weir (looks like a dam) (UTM E0375.8-N2140.98). We will examine exposures of eclogite on the west side of the stream and boulders of garnet peridotite (among other lithologies) as we proceed back down stream. To the east is Loma de Quita Espuela (985 m), the highest point in the area. To the west is Loma El Quemada (565 m).

At the weir. The freshest samples of eclogite come from the low outcrop just above the weir on the west side of Rio Cuaba (~25 m downstream from what looks like a natural waterfall, but if you look closely, you will see that it has been cemented, to created a "catchment"). Rounded boulders of the eclogite can also be found in the streambed. The eclogite has 3-5 mm subhedral porphyroblast of pink garnet in a light gray-green matrix of symplectite (Pl-Cpx). Garnet is separated from the matrix by a thin (0.5 mm) mantle of hornblende. Quartz makes up less than 5 modal % of the rock.

Proceeding downstream. Boulders of garnet peridotite (assemblage III) are first encountered near the mouth of a small tributary (Arroyo El Arroyasa), which enters Rio Cuaba from the east (~100 m downstream from the weir). Boulders of garnet peridotite can be traced up the arroyo to the east ~600 m. Farther upslope, the terrain is covered by landslide deposits. In the streambed of Rio Cuaba, boulders of garnet peridotite range in size up to 3 m. They are easy to recognize by the large (1-2 cm) phenocrysts of pink garnet. The assemblage is Cpx+Ol+Grt+Spl+(retrograde Hbl + Srp) (III, Fig. 2b). The garnets are mantled by pale gray-green clinopyroxene and late hornblende. The matrix consists of black, partially serpentinized olivine. Spinel occurs as minute (<0.5 mm) emerald green inclusions in the garnet. Locally, where olivine is scarce, the assemblage is Cpx+Grt+Spl+Crn (V). Other ultramafic assemblages (I, II, IV) have not been recognized in this part of the

drainage basin of Rio Cuaba. Boulders of the other assemblages (I, II, IV, V) occur mainly in the upper parts of the next two tributaries to the east (Arroyo Los Canos and Rio Los Bracitos).

Return to vehicle, and proceed to the main road, RD19.

13.0 Proceed **E** on RD19.

15.8 Turn left onto gravel road (~UTM E0378.3-N2137.9).

15.9 Park vehicle (~UTM E0378.3-N2139.7).

Stop 2, East branch, Arroyo Los Canos:
From the vehicle, proceed ~0.6 km **W** on foot (jeep trail) to a sharp turn to the right.
Proceed **NE** on this secondary jeep trail ~0.6 km to just past a farmhouse on the left.
Proceed north **N** ~0.5 km through pasture, easy going, to Arroyo Los Canos.
Proceed upstream (**NE**). The objective of this trek is a 5-m boulder of olivine clinopyroxenite at ~UTM E0378.5-N2139.2
The boulder is cut by a narrow (1-4 cm), straight dike of clinopyroxene garnetite. Because of its hardness and toughness, we have yet to obtain a good sample of this particular boulder. Olivine clinopyroxenite and the clinopyroxene garnetite have been sampled elsewhere from more amenable boulders. The dark greenish-gray olivine clinopyroxenite consists of Cpx+Ol+Opx+Mag+Cr-Spl+(late hornblende and serpentine) (I, Fig. 2a). The orthocumulate texture is defined by subhedral phenocrysts (~5 mm) of clinopyroxene, with olivine filling the interstices. Orthopyroxene occur as minute (~0.01 mm) euhedral inclusions in olivine. Weathering of the surface of the boulder produced low-amplitude corrugations with a wavelength of ~5 cm. The differential weathering reflects a subtle modulation in the modal proportions of olivine and clinopyroxene. We have suggested this modulation reflects rhythmic igneous layering, implying that the olivine clinopyroxenite crystallized from a convectively circulating magma in a well-developed magma chamber.

Garnet makes up more than 90% of the narrow dike, with rare but conspicuous 1-cm euhedral crystals of clinopyroxene. The mineral assemblage is Grt+Cpx+Spl+(late Hbl+Mag) (IV, Fig. 2a). Spinel occurs as fine (0.01-0.02 mm) inclusions in the garnet. Hornblende

forms 1-3 mm selvages at the margins of the dike, and also fills fractures in the garnet. The hornblende is interpreted as a product of late, retrograde hydration. Presumably the original intrusive contact served as a conduit for H_2O.

According the phase relationships (Fig. 4c), we interpret much of the garnet in the dike as having formed by the subsolidus breakdown of magmatic high-Al clinopyroxene (isochemical with garnet, or nearly so).

Return to the vehicle, and proceed to the main road, RD19.

16.0 Go right (**W**) on RD19.
18.8 Pass turn-off to Cuevas.
27.8 Intersection of RD132/RD19 in San Francisco de Macoris.

References
*Essential reading for the UHP – LP debate.

*Abbott, R.N., Jr., Broman, B.N & Draper, G. (2007) - UHP magma paragenesis revisited, olivine clinopyroxenite and garnet-bearing ultramafic rocks from the Cuaba Gneiss, Rio San Juan Complex, Dominican Republic. Int. Geol. Rev., 49, 572-586.

Abbott, R.N., Jr. & Draper, G. (1998) - Retrograde eclogite in the Cuaba Amphibolite of the Rio San Juan Complex, northern Hispaniola [abs.]. 15th Caribbean Geological Conference, Kingston, Jamaica.

Abbott, R.N., Jr. & Draper, G. (2002) -Retrograded eclogite in the Cuaba Amphibolite of the Rio San Juan Complex, Northern Hispaniola. In: Jackson, T.A. (Ed.). Caribbean geology: into the third millennium: Transactions of the 15th Caribbean Geological Conference. The University of the West Indies Press, Kingston, Ch. 8, 97-108.

*Abbott, R.N., Jr. & Draper, G. (2007) - Petrogenesis of UHP eclogite from the Cuaba Gneiss, Rio San Juan complex, Dominican Republic. Int. Geol. Rev., 49, 1069-1093.

Abbott, R.N., Jr. & Draper, G. (2008) - Evolution of garnet and clinopyroxene in UHP ultramafic rock, Cuaba Gneiss, Rio San Juan complex, Dominican Republic. Geol. Soc. Amer. Abstracts with Programs, 41(6), Abs. no.193-37, Houston.

*Abbott, R.N., Jr. & Draper, G. (2010) - Comments on "Corundum-bearing peridotite from northern Dominican Republic: a metamorphic product of an arc cumulate in the Caribbean subduction zone," by Hattori et al. [Lithos 114 (2010) 437-450]. Lithos, 117, 322-326.

*Abbott, R.N., Jr. & Draper, G. (2013) – The case for UHP conditions in the Cuaba terrane, Rio San Juan Metamorphic complex, Dominican Republic. Geologica Acta, 11, 149-165. doi: 10.1344/105.000001841.z

Abbott, R.N., Jr., Draper, G. & Broman, B.N. (2006a) - P-T path for ultra high pressure garnet ultramafic rocks of the Cuaba Gneiss, Rio San Juan Complex, Dominican Republic. Int. Geol. Rev., 48, 778-790.

Abbott, R.N., Jr., Draper, G. & Keshav, S. (2001) - Garnet peridotite found in the Greater Antilles. EOS (Trans. Amer. Geophys. Union), 82(35), 381-388.

*Abbott, R.N., Jr., Draper, G. & Keshav, S. (2005) - UHP magma paragenesis, garnet peridotite and garnet clinopyroxenite: An example from the Dominican Republic. Int. Geol. Rev., 47, 233-247.

*Abbott, R.N., Jr., Draper, G. & Keshav, S. (2006b) [*NOTE: This is a reprint of Abbott et al., 2005*] - UHP magma paragenesis, garnet peridotite and garnet clinopyroxenite: An example from the Dominican Republic. In: Liou, J. G. & Cloos, M. (Eds.), Phase relations, high-pressure terranes, P-T-ometry, and plate pushing: A tribute to W. G. Ernst. Bellwether Publishing, Ltd. for Geol. Soc. Amer., International Book Series, 9, 653-667.

Ackermand, D., Seifert, F. & Schreyer, W. (1975) - Instability of sapphirine at high pressure. Contrib. Mineral. Petrol., 50, 79-92.

Ai, Y. (1994) - A revision of the garnet-clinopyroxene Fe^{2+}-Mg exchange thermometer. Contrib. Mineral. Petrol., 115, 467-473.

Boyd, F.R. (1970) - Garnet peridotites and the system $CaSiO_3$-$MgSiO_3$-Al_2O_3. Mineral. Soc. Amer. Special Paper 3, 63-75.

Davidson, P.M. & Burton, B. (1987) - Order-disorder in omphacitic pyroxenes: A model for coupled substitution in the point approximation. Amer. Mineral., 72, 337-344.

Davidson, P.M. & Lindsley, D.H. (1985) - Thermodynamic analyses of quadrilateral pyroxenes. Part II: Model calibration from experiments and application to geothermometry. Contrib. Mineral. Petrol., 91, 390-404.

*De Hoog, J.C.M. (2012) - Comments on "Garnet-bearing ultramafic rocks from the Dominican Republic: Fossil mantle plume fragments in an ultra high pressure oceanic complex?" by Gazel et al. [Lithos 125 (2011) 393-404]. Lithos, 134-135, 330-334.

Draper, G., Abbott, R.N., Jr. & Keshav, S. (2002) - Indication of UHP metamorphism in garnet peridotite, Cuaba Unit, Rio San Juan Complex, Dominican Republic [abs.]. 16th Caribbean Geological Conference, Barbados.

Draper, G., Abbott, R.N., Jr. & Keshav, S. (2005) - Cuaba Gneiss, Dominican Republic: An ultra high pressure metamorphic terrane in the northern Caribbean [abs.]. 17th Caribbean Geological Conference, San Juan, PR.

Draper, G., Mann, P. & Lewis, J.F. (1994) - Hispaniola, In: Donovan, S.K. & Jackson, T.A. (Eds.), Caribbean Geology: An introduction. University of the West Indies Publishers' Association, Kingston, Jamaica, Ch. 7, 129-150.

Draper, G. & Nagle, F. (1991) - Geology, structure, and tectonic development of the Rio San Juan Complex, northern Dominican Republic. In: Mann P., Draper, G. & Lewis, J.F. (Eds.), Geologic and Tectonic development of the North American-Caribbean Plate Boundary in Hispaniola: Geol. Soc. Amer. Special Paper, 262, 77-95.

Draper, G., Gutierrez, G. & Lewis, J.F. (1996) - Thrust emplacement of the Hispaniola peridotite belt: Orogenic expression of the mid-Cretaceous Caribbean arc polarity reversal? Geology, 24, 1143-1146.

Eberle, W., Hirdes, W., Muff, R. & Pelaez, M. (1982) - The geology of the Cordillera Septentrional (Dominican Republic). In: Snow, W., Gil, N., Llinas, R., Rodriguez-Torres & R., Tavares, I. (Eds.), Transactions, 9th Caribbean Geological Conference: Santo Domingo, Dominican Republic, 1980, 619-632.

Escuder-Viruete, J. (2009) - Petrología y Geoquímica de Rocas Igneas y Metamorficas (I y II): Hojas de Rio San Juan, Guayabito, Salcedo, Gaspar Hernandez, Pimentel, Cabrera y Villa Riva. Informe Complementario al Mapa Geologico de la Republica Dominicana a E. 1:50.000. Sysmin Project, IGME-BRGM, Santo Domingo, 163 p.

Escuder-Viruete, J., Friedman R., Castillo-Carrion, M., Jabites, J. & Perez-Estaun, A. (2011) - Origin and significance of the ophiolitic high-pressure mélanges in the northern Caribbean convergent margin: Insights from the geochemistry and large-scale structure of the Rio San Juan metamorphic complex. Lithos, 127, 483-504.

Escuder-Viruete, J., Valverde-Vaquero, P., Rojas-Agramonte, Y., Gabites, J., Castillo-Carrion, M. & Perez-Estaun, A. (2013a) - Timing of deformational events in the Rio San Jaun complex: Implications for the tectonic controls on the exhumation of high=P rocks in the northern Caribbean subduction-accretionary prism. Lithos, 177, 416-435.

Escuder-Viruete, J., Valverde-Vaquero, P., Rojas-Agramonte, Y., Gabites, J., Castillo-Carrion, M. & Perez-Estaun, A. (2013b) – From intra-oceanic subduction to arc accretion and arc-continent collision: Insights from the structural evolution of the Rio San Juan metamorphic complex, northern Hispaniola. J. Structural Geol. 46, 34-56.

*Gazel, E., Abbott, R.N., Jr. & Draper, G. (2011) - Garnet-bearing ultramafic rocks from the Dominican Republic: Fossil mantle plume fragments in an ultra high pressure oceanic complex? Lithos, 125, 393-404.

*Gazel, E., Abbott, R.N., Jr. & Draper, G. (2012) - Reply to Comment on "Garnet-bearing ultramafic rocks from the Dominican Republic: Fossil mantle plume fragments in an ultra high pressure oceanic complex?" by Jan. C.M. De Hoog. Lithos, 134-135, 335-339.

Gerya, T.V., Stockert, B. & Perchuk, A.L. (2002) - Exhumation of high-pressure metamorphic rocks in a subduction channel: A numerical simulation. Tectonics, 21(6-6), 1056, doi: 10.1029/2002TC001406

Gerya, T.V. & Yuen, D.A. (2003) - Rayleigh-Taylor instabilities from hydration and melting propel 'cold plumes' at subduction zones. Earth Planet. Sci. Lett., 212, 47-62.

Gorczyk, W., Guillot, S., Gerya, T.V. & Hattori, K. (2007) - Asthenospheric upwelling, oceanic slab retreat, and exhumation of UHP mantle rocks: Insights from Greater Antilles. Geophys. Res. Lett., 34, L21309, doi: 10.1029/2007/GL031059

Graham, C.M. & Powell, R. (1984) - A garnet-hornblende geothermometer: calibration, testing, and application to the Pelona Schist, southern California. J. Metam. Geol., 2, 13-21.

*Hattori, K.H., Guillot, S., Saumur, B.-M., Tubrett, M.N., Vidal, O. & Morfin, S. (2010a) - Corundum-bearing garnet peridotite from northern Dominican Republic: A product of an arc cumulate in the Caribbean subduction zone. Lithos, 114, 437-450.

*Hattori, K.H., Guillot, S., Tubrett, M.N., Saumur, B.-M., Vidal, O. & Morfin, S. (2010b) - Reply to Comments on "Corundum-bearing garnet peridotites from northern Dominican Republic: A metamorphic product of an arc cumulate in the Caribbean subduction zone" by Richard N. Abbott and Grenville Draper. Lithos, 117, 327-330, doi: 10.1016/j.lithos.2010.03.007

*Hattori, K., Tubrett, M., Saumur, B.-M. & Guillot, S. (2009) - Subduction of shallowly formed arc cumulates: Evidence from clinopyroxene compositions of garnet peridotites in the Rio San Juan complex, northern Dominican Republic. Geophys. Res. Abs., 11, EGU2009-6237.

Herzberg, C., Raterron, P. & Zhang, J. (2000) - New experimental observations on the anhydrous solidus for peridotite KLB-1. Geochem. Geophys. Geosyst., 1(10), 1051, doi: 10.1029/2000GC000089

Hays, J.F. (1966) - Lime-alumina-silica. Carnegie Institute of Washington Year Book 65, 234-239.

Hirschmann, M.M. (2000) - Mantle solidus: Experimental constraints and effects of peridotite composition. Geochem. Geophys. Geosyst., 1(10), 1042, doi: 10.1029/2000GC000070

Holland, T.J.B. & Powell R. (1998) - An internally consistent thermodynamic data set for phases of petrologic interest. J. Metam. Geol., 16, 309-343.

Jansma, P.E., Mattioli, G.S., Lopez, A., DeMets, C., Dixon, T.H., Mann, P. & Calais, E. (2000) - Neotectonics of Puerto Rico and the Virgin Islands, northeastern Caribbean, from GPS geodesy. Tectonics, 19, 1021-1037.

Kerr, A.C., White, R.V., Thompson, P.M.E., Tarney, J. & Saunders, A.D. (2003) - No oceanic plateau – no Caribbean plate? The seminal role of an oceanic plateau in Caribbean plate evolution. In Bartolini, C., Buffler, R.T. & Blickwede, J. (Eds.), The Circum Gulf of Mexico and Caribbean: Hydrocarbon Habitats, Basin Formation, and Plate Tectonics, Amer. Assoc. Petrol. Geol. Mem., 79, 126-268.

Keshav, S., Sen, G. & Presnall, D.C. (2007) - Garnet-bearing Xenoliths from Salt Lake Crater, Oahu, Hawaii: High-Pressure Fractional Crystallization in the Oceanic Mantle. J. Petrol., 48, 1681-1724.

Krebs, M., Maresch, W.V., Schertl, H.-P., Munker, C., Baumann, A., Draper, G., Idleman, B. & Trapp, E. (2008) - The dynamics of intra-oceanic subduction zones: A direct comparison between fossil petrological evidence (Rio San Juan Complex, Dominican Republic) and numerical simulation. Lithos, 103, 106-137.

Krebs, M., Schertl, H.P., Maresch, W.V. & Draper, G. (2011) - Mass flow in serpentine-hosted subduction channels: P-T-t path patterns of metamorphic blocks in the Rio San Juan mélange (Dominican Republic). J. Earth Sci., 42, 569-595.

Kretz, R. (1983) - Symbols for rock-forming minerals. Amer. Mineral., 68, 277-279.

Lewis, J.F. & Draper, G. (1990) - Geology and tectonic evolution of the northern Caribbean region, In: Dengo, G. & Case, J.E. (Eds.), The Caribbean Region: Boulder, Colorado, Geol. Soc. Amer., Geology of North America, H, 77-140.

Lieberman, J.E. & Till, A.B. (1987) - Possible crustal origin of garnet lherzolite: Evidence from the Kigluaik Mountains, Alaska. Geol. Soc. Amer. Abstracts with Programs, 19(7), 746.

Mann, P., Calais, E., Ruegg, J.-C., DeMets, C., Jansma, P.E. & Mattioli, G.S. (2002) - Oblique collision in the northeastern Caribbean from GPS measurements and geological observations. Tectonics, 21(6-7), 1057, doi: 10.1029/2001TC001304

Mann, P., Schubert C. & Burke, K. (1990) - Review of Caribbean neotectonics, In: Dengo, G. & Case, J.E. (Eds.), The Caribbean Region: Boulder, Colorado, Geol. Soc. Amer., Geology of North America, H, 307-338.

MacKenzie, J.M., Canil, D., Johnston, J.E., English, J., Mihalynuk, M.G. & Grant, B. (2005) - First evidence for ultrahigh-pressure garnet peridotite in the North American Cordillera. Geology, 33, 105-108.

Milholland, C.S. & Presnall, D.C. (1998) - Liquidus phase relations in the CaO-MgO-Al_2O_3-SiO_2 system at 3.0 GPa: the aluminous pyroxene thermal divide and high-pressure fractionation of picritic and komatiitic magmas. J. Petrol., 39, 3-27.

Parkinson, C.D., Motoki, A., Onishi, C.E. & Maruyama, S. (2001) - Ultrahigh-pressure pyrope-kyanite granulites and associated eclogites in Neopreterozoic nappes of Southeast Brazil. UHPM Workshop 2001, Fluid/slab/mantle interactions and ultrahigh-P minerals. Waseda Univ., Tokyo, Abstract Volume, 87-90.

Pindell, J.L. & Barrett, S.F. (1990) - Geological evolution of the Caribbean region; a plate tectonic perspective. In: Dengo, G. & Case, J.E. (Eds.), The Caribbean Region: Boulder, Colorado, Geol. Soc. Amer., Geology of North America, H, 405-432.

Pindell, J. & Kennan, L. (2009) - Tectonic evolution of the Gulf of Mexico, Caribbean and northern South America in the mantle reference frame: an update. In Lorente, J.K. & Pindell, J. (Eds.), The Geology and Evolution of the region between North and South America: Geol. Soc. London, Special Publication, 328, 1-55.

Pindell, J., Kennan, L., Maresch, W.V., Stanek, K-P, Draper, G. & Higgs, R. (2005) - Plate-kinematics and crustal dynamics of circum-Caribbean arc-continent interactions and tectonic controls on basin development. In: Avé Lallemant, H. G. & Sissons V. B. (Eds.), Proto-Caribbean margins, in Caribbean - South American plate interactions, Venezuela. Geol. Soc. Amer. Special Paper 394, 7-52, doi: 10.1130/2005.2394(01)

Powell, R. (2005) - THERMOCALC, (v. tc325) web site http://www.earthsci.unimelb.edu.au/tpg/thermocalc/.

Powell, R., Holland, T.J.B. & Worley, B.A. (1998) - Calculating phase diagrams involving solutions via on-linear equations, with examples using THERMOCALC. J. Metam. Geol., 16, 577-588.

Roselle, G.T., Thuring, M. & Engi, M. (2002) - MELONPIT: A finite element code for simulating tectonics mass movement and heat flow within subduction zones. Amer. J. Sci., 302, 381-409.

Sen, G., Keshav, S. & Bizimis, M. (2005) - Hawaiian mantle xenoliths and magmas: Composition and thermal character of the lithosphere: Amer. Mineral., 90, p. 871–887.

Schmidberger, S.S. & Francis, D. (2001) - Constraints on the trace element composition of the Archean mantle root beneath Somerset Island, Arctic Canada. J. Petrol., 42, 1095-1117.

Spear, F.S. (1993) - Metamorphic Phase Equilibria and Pressure-Temperature-Time Paths: Mineral. Soc. Amer. Monograph, Washington, 799 p.

Sun, S. & McDonough, W.F. (1989) - Chemical and isotopic systematics of oceanic basalts: Implications for mantle composition and processes. In: Saunders, A.D. & Norry, M.J. (Eds.), Magmatism in ocean basins. Blackwell Scientific, Boston, 313-345.

Till, A.B. (1981) - Alpine-type garnet lherzolite of the Kigluaik Mountains, Seward Peninsula, Alaska. Geol. Soc. Amer. Abstracts with Programs, 13 (2), 110.

Tuff, J. & Gibson, S.A. (2007) - Trace-element partitioning between garnet, clinopyroxene and Fe-rich picritic melts at 3 to 7 GPa. Contrib. Mineral. Petrol., 153, 369–387, doi: 10.1007/s00410-006-0152-x

Walter, M.J. (1998) - Melting of garnet peridotite and the origin of komatiite and depleted lithosphere. J. Petrol., 39, 29-60.

Wei, C.J. & Clarke, G.L. (2011) - Calculated phase equilibria for MORB compositions: a reappraisal of the metamorphic evolution of lawsonite eclogite. J. Metam. Geol., 29, 939-952.

Whitney, D.L. & Evans, B.W. (2010) - Abbreviations for names of rock-forming minerals. Amer. Mineral., 95, 185-187.

Zhang, R.Y., Liou, J.G. & Zheng, J.P. (2004) - Ultrahigh-pressure corundum-rich garnetite in garnet peridotite, Sulu terrane, China. Contrib. Mineral. Petrol., 147, 21-31.